Measuring the Scale of Segregation in Mixing Data

Alena Kukukova,[1] Joelle Aubin[2] and Suzanne M. Kresta[1]*

1. *Department of Chemical and Materials Engineering, University of Alberta, Edmonton, Alberta, Canada T6G 2G6*
2. *Laboratoire de Génie Chimique CNRS/INPT/UPS, Université de Toulouse, 4 Allée Emile Monso, BP-84234, 31030 Toulouse Cedex 4, France*

Four methods were used to extract length scales from mixing data: the maximum striation thickness, point-to-nearest-neighbour (PNN) distributions, the correlogram and the variogram. Four test data sets were analysed: blending in a micromixer; particle dispersion in a stirred tank; dispersion of a smoke plume and a pulse tracer test in a reactor. The maximum striation thickness captures the largest length scale. The PNN method quantifies differences between clustered, random and regular spatial distributions. The correlogram calculation cannot be consistently used for all types of mixing data and has therefore been rejected. The variogram reveals both large-scale segregation and periodicity. Sub-sampling is needed to isolate smaller structures. The variogram, PNN and transect methods all successfully extracted mixing length scales from large 2D data sets.

Keywords: mixing length scales, scale of segregation, striation thickness, variogram, point-to-nearest-neighbour

INTRODUCTION

The scale of segregation is one of three measures of mixing defined by Kukukova et al. (2009). The scale of segregation is important for laminar mixing where the maximum striation thickness determines product quality, and for multi-phase mixing where the size of the particles drops and bubbles either determines mass transfer rates, or is the main objective of the operation. Industrial examples where the scale of segregation is the primary process objective are the formation of emulsions of a specified drop size (Atiemo-Obeng and Calabrese, 2004; Liu et al., 2005; Chu et al., 2007), the production of nanoparticles (Johnson and Prud'homme, 2003), the deliberate use of micromixing to reduce both the quantity of chemicals used and the environmental impact of the pulp and paper industry (Bennington, 2004), or to maximise reaction yield in mixing sensitive reactions (Bałdyga and Bourne, 1999), or to minimise NO_x emissions from rotary kilns (Newbold et al., 2000; Nathan et al., 2006). In all of these processes, the scale of segregation is the determining variable in the process. A simple illustration of the reduction of the scale of segregation as mixing progresses is shown in Figure 1.

A survey of the literature shows that the scale of segregation is important in a surprisingly wide spectrum of disciplines and a number of methods for its calculation have been proposed. The concept of the scale of segregation in engineering was introduced by Danckwerts (1952). He suggested the calculation of a mean length scale based on the correlogram—a plot of the coefficient of correlation of concentration, or concentration autocorrelation, versus the distance separating the data points. The scale of segregation based on autocorrelation was revisited by Lacey and Mirza (1976). At that time, the calculation was not deemed practical because of the large number of data pairs that have to be measured and analysed in order to get meaningful results. Due to the exponential increase of computer power and the increasing resolution and accessibility of digital images, the correlogram and related calculation methods are now practical for the analysis of quite common experimental data sets.

The scale of segregation can also be represented by the physical thickness of striations in a mixing field. In polymer processing applications, Mohr et al. (1957) developed a relationship between striation thickness and shear rate. Later, Muzzio et al. (1991) used a model mixing field with several million tracer particles to study the relationship between the striation thickness distribution and the stretching distribution. While the stretching distribution is the

*Author to whom correspondence may be addressed.
E-mail address: suzanne.kresta@ualberta.ca

Figure 1. The classical checkerboard problem. The scale of segregation decreases from left to right while the intensity of segregation stays the same.

more mathematically transparent approach because it is directly related to the shear field, the striation thickness distribution is the result needed for engineering design. They were able to show that the stretching distribution and the striation thickness distribution are directly coupled and inversely proportional, so that the striation thickness distribution can be directly calculated from the stretching distribution. If the stretching distribution can be calculated from the velocity field, the need to track millions of tracer particles in order to resolve the finest striations can be eliminated. When resolution of the finest scales of mixing is required, this can significantly reduce the computational requirements for a numerical solution. When macroscale segregation is the variable of interest, a small number of tracer particles can be used and the maximum striation thickness can be determined along a single reference transect. The maximum striation thickness on a transect is an important measure of equipment performance and product quality in laminar mixing (Aubin et al., 2005).

There is also a well-developed literature on segregation problems and measures of segregation in population ecology, geostatistics, segregation of minority populations, forestry, medical imaging and basic applied statistics. These data take the form of locations of members of a population at an instant in time, resulting in a spatial point pattern. A number of distance methods for analysing spatial point patterns which were developed in the American forestry literature (Cottam and Curtis, 1949) are based on the distribution of distances between neighbours (Diggle, 2003). Three methods for analysing spatial point patterns are identified in the spatial statistics literature. Since all of the spatial point patterns in this paper are made up of tracking particles, and the particles are located within a set of grid points, we refer to the data as particles and the grid points as points. The first method analyses all inter-particle distances within a population; the second calculates the distribution of distances between each particle and its nearest neighbour and the third and most common method measures the distance from a set of grid points to the nearest particle (point-to-nearest-neighbour (PNN) method). The spatial distribution of the population is evaluated by comparing the nearest neighbour distribution to a completely random Poisson distribution. When the PNN distribution is random, the match with the Poisson distribution is close, and when clustering is present, the distribution is distorted. Spatial point patterns have only recently been used to assess the scale of segregation and the quality of mixing (Aubin et al., 2005; Kukuková et al., 2008).

Carle and Fogg (1996) evaluated the mean length scale in geostatistics using variograms, which quantify the spatial correlation of data based on the variance between data versus the distance separating them. A similar approach is to use the variance of the average of several contiguous concentrations (Gullett et al., 1993). Although the variogram is used primarily for modelling when only limited data are available (Deutsch, 2002), this calculation also appears useful for the analysis of dense data sets. The variogram is closely related to the Danckwerts correlogram (1952). Correlograms and variograms both show the spatial variability or continuity of the underlying data set. The resulting curves can reveal both large-scale segregation and periodicity in the data. Correlograms and variograms also allow the calculation of length scales. The scale of segregation can be evaluated in several directions of interest or, if all data are combined together, an average length scale of the whole field can be obtained.

The authors' previous work (Kukukova et al., 2009) presents an introduction into the three dimensions of segregation, their definitions and possible applications. A second paper (Kukuková et al., 2008) explores the first dimension—the intensity of segregation—in detail and focuses on accurate sampling strategies. This work concentrates on the second dimension—the scale of segregation. In this study, four methods of measuring the scale of segregation were considered for application to mixing data: the maximum striation thickness on a transect, PNN distribution, the correlogram and the variogram. The methods are compared to determine their strengths and limitations for the analysis of mixing data. Five questions are of interest when evaluating the four measures:

1. What type of data is the method suitable for?
2. What information does it provide?
3. Are the results physically meaningful?
4. What is the smallest scale of mixing resolved by the method?
5. How fast is the calculation?

While conditions 1 and 5 have straightforward answers, the other questions require testing and illustration with representative data sets. The goal of this work is to provide a toolkit of fast methods for length scale characterisation, as well as benchmarks for the proper use and limitations of each tool. In the next section, each of the methods is discussed in detail.

METHODS

This section will review the four methods chosen to measure the scale of segregation: the maximum striation thickness on a transect, the PNN distributions, the correlogram and the variogram. The four test cases are presented after this section, and details about the practical application of the methods to the test cases are given in the Results and Discussion Section. Calculation algorithms for all of the methods are available as supplementary material from the Journal or on request to the corresponding author.

Maximum Striation Thickness on a Transect

For spatial point patterns, the maximum striation thickness on a transect can be evaluated using inter-particle distances (Aubin

Figure 2. Example of transect sampling in a plane of data.

et al., 2005). In such applications, a transect through a data plane or volume is chosen and the distance between two consecutive particles lying on the transect is measured. The inter-particle distances are then compared with a threshold value to determine if they are part of the same striation or not. A distribution of striation thicknesses is obtained and the thickness of the largest striation can be found. The latter is a measure of the limiting scale of segregation.

To get the most valuable information about mixing, a transect should pass through the worst mixed part of the mixing field, and should be perpendicular to the striations of greatest interest, as shown in Figure 2. Transects are of zero thickness mathematically, but numerically, a finite thickness is required to sample a statistically and physically meaningful number of particles. A transect has two variable dimensions: the height of the transect, Δz, and the particle separation threshold Δx. A particle is included in the transect if its z-coordinate equals the z-coordinate of the transect $\pm\Delta z/2$. Aubin et al. (2005) recommend a transect height, Δz, equal to the mean particle spacing in the mixing field. The height of the transect, Δz, allows for the capture of a single particle so that all particles in the 2D transect are associated with the equivalent 1D line through the mixing field. The striation thicknesses on the transect are determined using the function f, which has the following properties:

$$\begin{aligned} &\Delta x(\text{neighbours}) \leq \Delta x : f(x) = 1 \\ &\Delta x(\text{neighbours}) > \Delta x : f(x) = 0 \end{aligned} \tag{1}$$

Striation thicknesses on the transect are calculated directly from the function $f(x)$: when two consecutive particles in the transect are within Δx of each other, they are both in the same striation. If Δx is too large, the striations will be unrealistically large; if it is too small, no striations will be detected. In our previous work (Kukuková et al., 2008), several transect heights, Δz, and striation thickness thresholds, Δx, were studied. It was concluded that a value of $\Delta x = \Delta z$ equal to the mean particle spacing gives the best resolution.

Point-to-Nearest-Neighbour Distributions

The PNN method measures the distance x_i from each of m grid points to the nearest of the n particles, as illustrated in Figure 3. In fields of demography, ecology, geography and forestry, these distance data are analysed using a test of complete spatial randomness (CSR). The CSR hypothesis asserts that for a completely random distribution of particles in region A, any particle has an

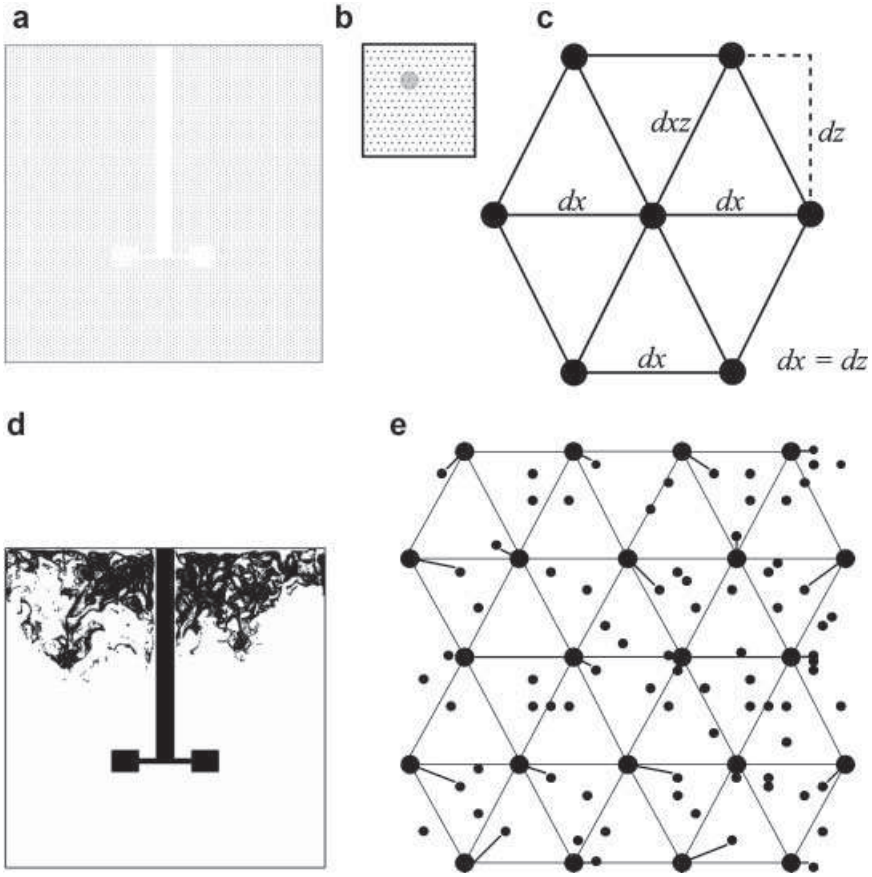

Figure 3. Illustration of the PNN method: (a) Hexagonal grid in a stirred tank. (b) Enlarged grid. (c) Construction of the base unit of the grid. (d) Particle locations in the tank. (e) Search for nearest neighbours of each grid point.

equal probability of being at any position in region A and the position of any particle is independent of the position of any other particle. If the particles are randomly distributed in space, the PNN distances should follow a Poisson distribution. Deviations from the random Poisson distribution allow regular and clustered spatial patterns to be distinguished.

For PNN measurement on a plane of data, m grid points are arranged in a regular $k \times k$ grid. Diggle and Matern (1980) recommend using a number of grid points equal to the number of tracking particles, giving $k \approx \sqrt{n}$. Using a grid that is well matched to the number of particles maximises the use of each particle in the analysis, and also optimises the resolution of the PNN distribution. The most uniform pattern for a set of points occurs in a regular hexagonal lattice. The mean grid spacing, x_G, for the hexagonal lattice shown in Figure 3c is:

$$x_G = \frac{2dx + 4dxz}{6} \cong 1.08dx \tag{2}$$

where dx is the horizontal spacing, $dx = dz$ and dxz is the diagonal grid spacing. When the number of grid points is matched to the number of particles, x_G also approximates the spatial resolution of the measurement.

Clustering can be qualitatively evaluated from the shape of the PNN distribution. A wide distribution indicates clustering; a narrow distribution corresponds to a regular spatial distribution of particles. Another indicator that the particles are well mixed is the mean PNN distance $\bar{x}_i$. As the PNN distribution approaches perfect homogeneity, $\bar{x}_i$ approaches the point–particle distance for a perfectly homogeneous distribution.

A more quantitative measure of clustering and departure from CSR is the index of dispersion, I_{disp} (Diggle, 2003), which is the ratio between the variance of the PNN distribution and the mean of the distribution:

$$I_{disp} = \frac{\sigma^2}{\overline{x_i}} \tag{3}$$

Because the Poisson distribution has a variance equal to its mean, the index of dispersion will be equal to 1 for a random distribution, larger than 1 for a clustered distribution and smaller than 1 for a regular distribution of particles.

A filtered variance of the PNN distribution can be used to evaluate the deviation of the spatial arrangement of particles with respect to the expected homogeneous distribution defined by the grid points. A filter threshold, x_R is imposed such that at any value of $x_i < x_R$, the particle is considered to be close enough to the grid point and x_i is assigned a value to x_R. A variance of zero corresponds to the situation where the nearest neighbours of all grid points lie inside virtual circles with a radius of x_R and centred at grid points, thereby lying close enough to the grid points to be considered homogeneously distributed. The filtered point–particle variance is given by:

$$\sigma_R^2 = \frac{1}{m-1} \sum_{i=1}^{m} (x_i - x_R)^2 \quad \text{where } x_i = x_R \text{ if } x_i < x_R \tag{4}$$

The choice of x_R depends on the scale of interest but is limited by the resolution of the sampling grid, which is in turn dependent on the number of particles. The maximum meaningful value of x_R is one half of the mean grid spacing x_G, in order not to have overlapping filter areas. As x_R decreases, the homogeneous criterion becomes stricter.

Correlograms and Variograms

The correlogram probes the underlying structure in the data by plotting the coefficient of correlation versus the distance separating data points. For concentration data, the coefficient of correlation is given by:

$$R_x(h) = \frac{1/(N(h)) \sum_{N(h)} (C_i(x) - \bar{C})(C_i(x+h) - \bar{C})}{\sigma^2} \tag{5}$$

where $N(h)$ is the total number of pairs of data separated by distance h, and $\bar{C}$ and σ^2 are the mean and variance of the full 2D data set.

The variogram is calculated from:

$$\gamma x(h) \equiv \frac{1}{2N(h)} \sum_{N(h)} (C_{is}(x) - C_{is}(x+h))^2 \tag{6}$$

where C_{is} is the standardised concentration value at location x, which is the concentration centred with the mean and normalised with the standard deviation:

$$C_{is}(x) = \frac{C_i(x) - \bar{C}}{\sigma} \tag{7}$$

The variogram is closely related to the coefficient of correlation. For data where the mean and the variance of the population do not change with sample location, the following relationship holds:

$$\gamma_x(h) = 1 - R_x(h) \tag{8}$$

This equation will not hold exactly for data with large-scale segregation because the mean and variance of the data will vary with location in the field and the normalising of the data occurs in a different order for the correlogram and the variogram. For these situations, the two measures should be calculated separately.

The coefficient of correlation and variogram are very similar. Both are performed for a number of separation distances, with a maximum distance equal to about the half of the studied field in order to have enough pairs to statistically represent the entire field. The correlogram and variogram curves can be obtained for several directions of interest to reveal directional anisotropy. If the number of available data points is very small, all directions can be combined in one omni-directional plot, creating a picture of average spatial correlation or variability in the mixing field.

A comparison of the correlogram and the variogram is shown in Figure 4. The coefficient of correlation is always one at zero separation distance, which means that the concentration is perfectly correlated with itself, and falls towards zero as the separation distance increases. A value of zero indicates no correlation. If the correlogram crosses zero and reaches negative values, as shown in Figure 4, there is large-scale segregation. The variogram shape is exactly opposite to the correlogram. Variograms start with a value of zero at zero separation distance, meaning there is no variability. The curve then increases towards one, and sometimes exceeds it. A variogram equal to one means that the variability at h has reached the variance of the whole data set and there is no remaining spatial correlation in the data. Similar to the correlogram, when the variogram increases beyond one, there is large-scale segregation. Periodic oscillations in both the correlogram and variogram plots indicate underlying periodicity in the data.

If good mixing is characterised as the random spatial distribution of concentrations, the correlogram of a perfectly mixed

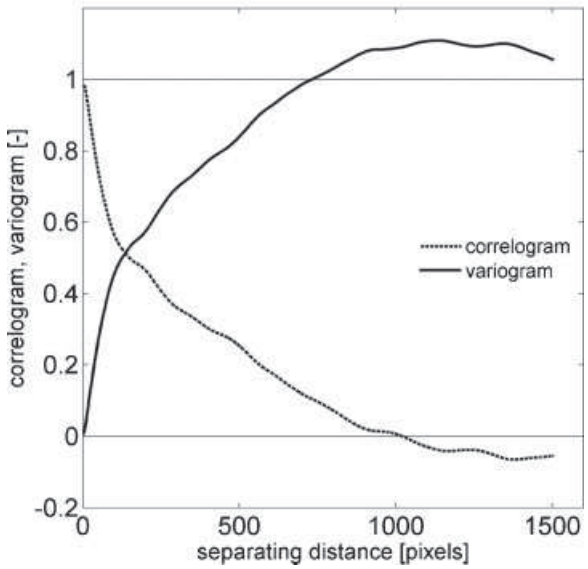

Figure 4. Comparison of the correlogram and the variogram for a representative sample of the smoke data.

population will drop to zero for all separation distances bigger than zero, showing there is no correlation in the data. Similarly, the variogram will rise instantly to one for separation distances bigger than zero, indicating that the variability everywhere is equal to the overall data variance.

Integration of the correlogram curve from $h=0$ to the point where the coefficient of correlation R_x equals zero gives a mean length scale (Danckwerts, 1952):

$$L_{\mathrm{D}} = \int_0^{\xi} R_x(h)\mathrm{d}h \tag{9}$$

as shown in Figure 5a. The length scale obtained in this calculation is not the exact size of clumps or clusters but an average over the mixing field. Danckwerts specified that this calculation should only be used for data with no large-scale segregation and no periodic patterns, giving correlograms that are always positive and non-periodic. In the context of today's mixing research, this seems unrealistic.

For variograms, a more flexible length scale calculation was proposed by geostatisticians Carle and Fogg (1996), who evaluated the mean length scale from the inverse of the initial variogram slope:

$$L_V = \left[\frac{\partial \gamma_x}{\partial h}\right]^{-1}_{h\to 0} P \tag{10}$$

as illustrated in Figure 5b. In this calculation, P is the proportion of the minor species in the sample region. They showed that the resulting scale of segregation is proportional to the average length scale in the sample region. The reasoning behind this calculation is the following: if we place the origin at the centre of an average-sized blob of diffusive tracer in the field and move from the origin toward the blob boundaries and to the surroundings, the variability of concentration will increase much faster for small blobs due to the jump of concentration at the boundaries and slower for bigger blobs. This length scale calculation can be performed for all kinds of data and variogram plots, regardless of oscillations or large-scale segregation.

TEST CASES

Two types of data were used for the scale of segregation measurements: particle tracking data, and concentration field data. The particle tracking data provide spatial point patterns where the locations of discrete particles, or members of a population, are known. The second data type is concentration maps, also called lattice data because the data values are available for a complete lattice of points. In digital images, the lattice is made up of pixels. Two data sets of each type were used to evaluate the measurement methods. The first test case is the laminar mixing of mass-less tracer particles in a staggered herringbone micromixer, shown in Figure 6. The second test case is the dispersion of floating particles in a turbulent stirred tank, shown in Figure 7. The third test case is the dispersion of smoke in a wind tunnel for a range of laminar to turbulent flow regimes, shown in Figure 8. The last test case is a concentration step change experiment in a continuous flow industrial reactor geometry, shown in Figure 9. In the first two cases, CFD provided complete 3D data sets and planes of data were extracted for analysis. In the third and fourth test cases, planar experimental data from digital images was used. While only 2D data sets were analysed in this work, the extension of the calculations to 3D analysis is straightforward.

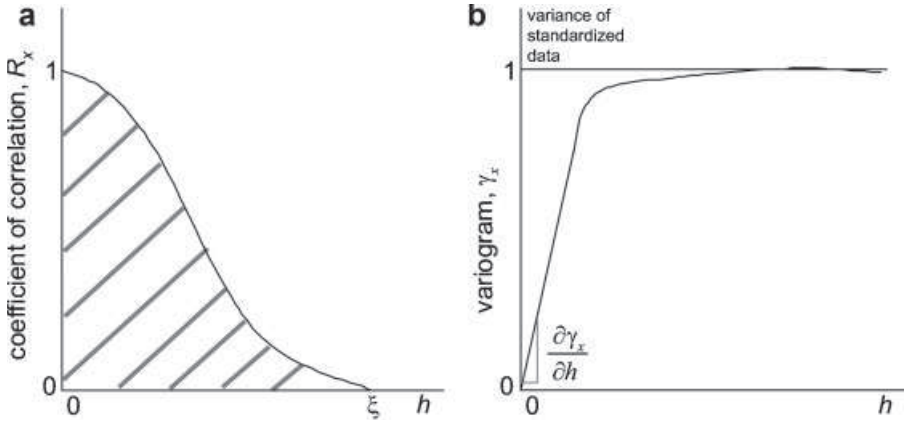

Figure 5. Length scale calculation from the correlogram and variogram: (a) Mean length scale evaluated as the area under the correlogram curve. (b) Sample variogram length scale proportional to the inverse of the initial slope.

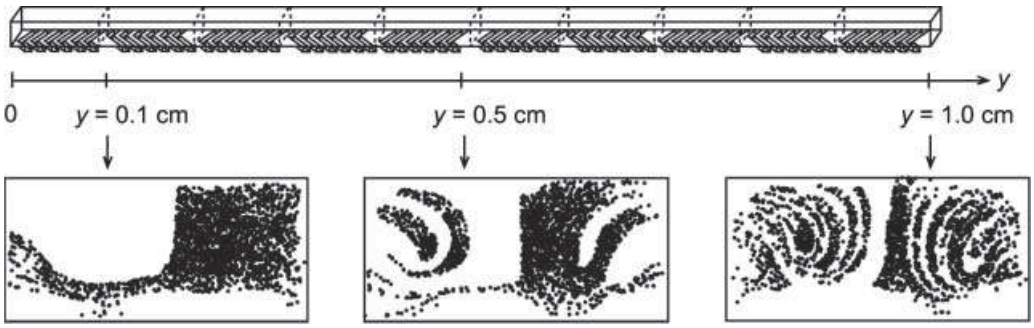

Figure 6. Staggered herringbone micromixer geometry and sample data for 2480 tracer particles and 10 mixer elements.

Detailed specifications of the first and second test cases are described in Aubin et al. (2005); and Hartmann et al. (2006), so only a brief summary is given here. For the herringbone micromixer shown in Figure 6, a total of 2480 uniformly distributed mass-less particles were placed on the right hand side of the solved flow field at the mixer inlet and were followed using the Lagrangian particle tracking method. Vertical planes along the micromixer were sampled at intervals of 100 μm to be used for analysis. The geometry used was the reference geometry with a width $W = 200\,\mu$m, height $H = 77\,\mu$m, groove depth $d_g = 0.23H$ and groove width $w_g = 50\,\mu$m.

The second test case is the dispersion of floating particles suspended in a baffled tank stirred by a Rushton turbine, shown in Figure 7. In this simulation, 7×10^6 mono-disperse spherical particles were tracked during a transient large eddy simulation. The data extracted from the simulation are the particle positions in a vertical cross-section mid-way between two baffles at six different times during the simulation.

The third test case is a jet in cross-flow forced with a synthetic jet of increasing strength (Watson, 2007; Watson and Sigurdson, 2008), as shown in Figure 8. In these experiments, a pipe with outer diameter $D_{pipe} = 2.54$ cm was inserted in a rectangular 30.5×30.5 cm wind tunnel with a turbulence intensity of 16%. Inside the outer pipe, an inner pipe of 20.6 mm was inserted, through which a jet flow was introduced at a range of Reynolds numbers, Re_d. This flow was further controlled and modified by velocity oscillations in the annular flow between the two pipes. This resulted in a 'synthetic jet' in different flow regimes spreading from the pipes into the wind tunnel. More experimental details can be found in Watson (2007); and in Watson and Sigurdson (2008). To visualise the flow, either the jet or the cross-flow was seeded with a glycerol and water based fog vapour, giving

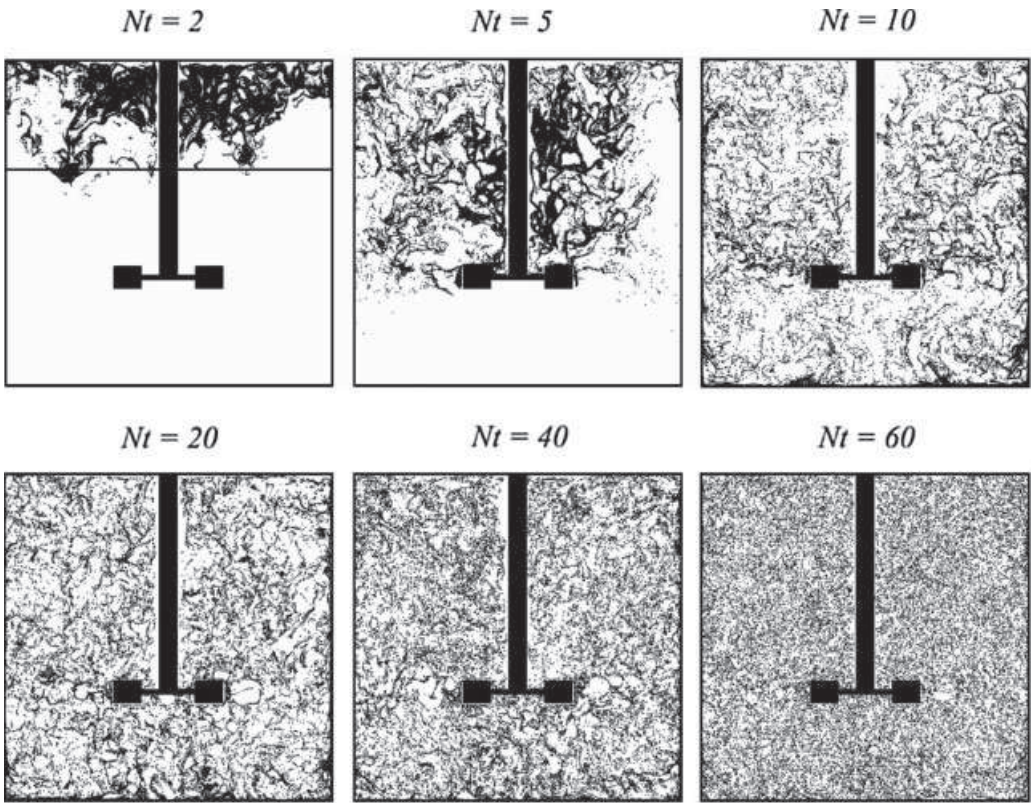

Figure 7. Stirred tank particle tracking data; $T = 0.2335$ m, $D = T/3$, impeller off-bottom clearance $C_{imp} = T/3$; 7×10^6 particles; Nt = number of impeller rotations.

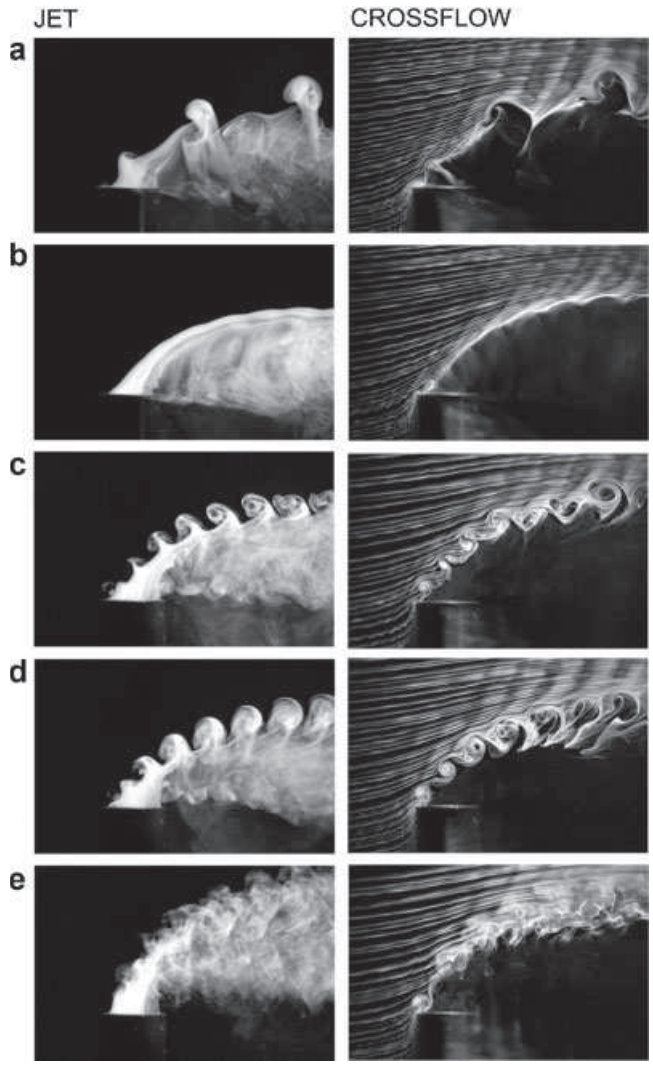

Figure 8. Jet in cross-flow photographs of different flow regimes: (a) Free jet, $Re_d = 570$. (b) Relaminarised jet, $Re_d = 660$. (c) Flow with upstream-pointing vortex structures, $Re_d = 1130$. (d) Flow with downstream-pointing vortex structures, $Re_d = 1130$. (e) Turbulent jet, $Re_d = 1500$. The flow is visualised by seeding the jet flow (pictures on the left) and the cross-flow (pictures on the right) with smoke. The image size is 3008×1960 pixels.

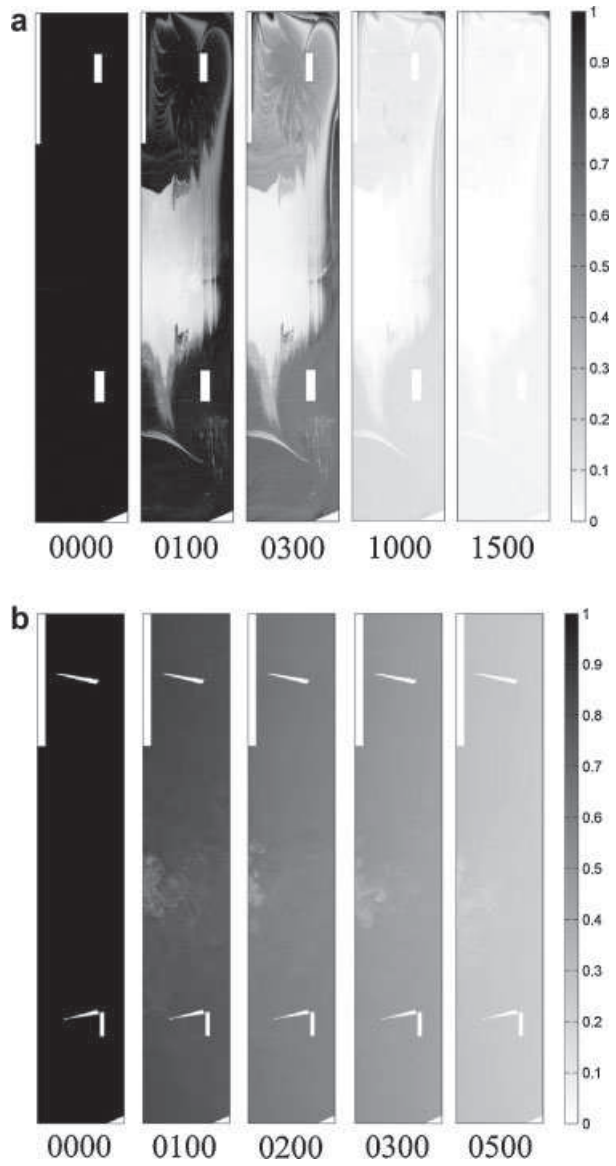

Figure 9. Reactor concentration data for two Reynolds numbers with the frame numbers shown below the images: (a) $Re = 17$. (b) $Re = 1478$. The average image size is 1290×225 pixels.

two photographs for each configuration. The 3008×1960 pixel greyscale images were analysed based on the greyscale intensity of the pixels corresponding to the smoke concentration.

The fourth data set is concentration maps of a glycerine–water mixture in a continuous flow industrial stirred tank reactor. The reactor is filled with dyed fluid at the beginning of the experiment. At time zero, a clear fluid is introduced into the reactor, mixing with and continuously washing out the dyed fluid. The feed location is on the side of the reactor and the exit is at the top. The experiment was performed for a range of Reynolds numbers from laminar to high transitional: $Re = 17$, 165, 1478 and 4498. The fluorescent dye is illuminated by a laser sheet and images of the reactor are captured by a camera as the experiment progresses. The image dimensions are approximately 1290×225 pixels. The resulting data are normalised tracer concentration measurements at each pixel. The concentrations of the tracer fluid change from 1 at the beginning to 0 when all the dyed fluid is washed out. Several image frames from the experiments are shown in Figure 9. Before further processing, the experimental data were filtered to eliminate the Gaussian white noise coming from the camera.

RESULTS AND DISCUSSION

The four methods of measuring the scale of segregation were applied to the four test cases and the results are discussed with respect to the five criteria defined in the introduction. First, the suitability of the methods for either point pattern or concentration data is noted. For each method, the practical considerations for application to the test cases are given, together with directions and suggestions on the best settings to use. This is followed by a comparison of the results of the length scale analysis with the scales visualised in the images and the physical meaning of the calculated scales is discussed. The conclusions for each method summarise the results of the evaluation criteria. Finally, the speed of the calculations for each method is compared at the end of the section.

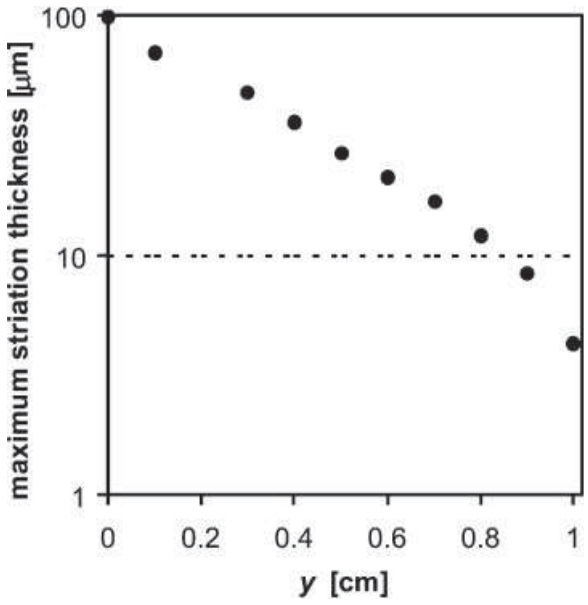

Figure 10. Maximum striation thickness as it decays along the micromixer.

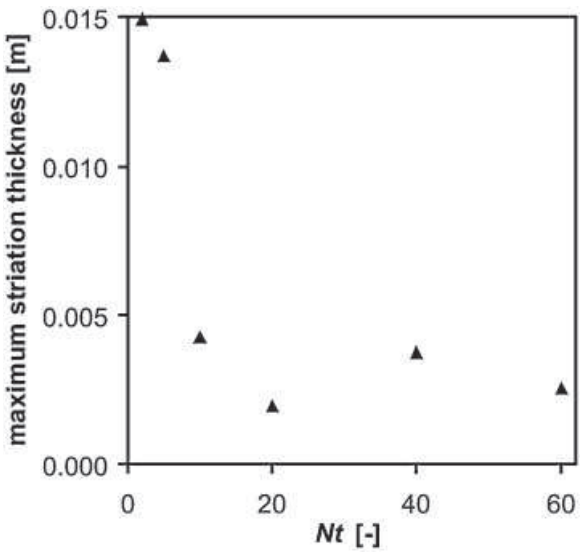

Figure 11. Maximum striation thickness on a transect in the stirred tank; Nt = number of time steps.

Maximum Striation Thickness on a Transect

Transect sampling is suitable for both point and concentration data. It was used to determine the maximum striation thickness in the micromixer, stirred tank and the smoke test cases.

For the staggered herringbone micromixer, the transect was located at mid-height of the microchannel, as illustrated in Figure 2, and the striation thickness calculation was performed using a resolution of $\Delta z = \Delta x = 5$ μm, which is equal to the mean particle spacing.

The calculated maximum striation thickness along the micromixer is shown in Figure 10. The width of the largest striation decreases exponentially as the fluid passes along the mixer. This is characteristic of chaotic flows as the flow is divided and reoriented at each element in the mixer, so the number of striations is expected to increase as K_0^n, where K_0 is the number of times the fluid is divided in each mixer element and n is the number of elements (Etchells and Meyer, 2004). As the number of striations increases, the CoV and the maximum striation thickness will necessarily decrease, but the rate of decrease cannot easily be predicted from the mixer geometry. In the laminar micromixer, volume filling and scale reduction happen simultaneously and the decay in the maximum striation thickness is a smooth curve. Based on the slope of the curve in Figure 10, K_0 is estimated to be 1.33. Using this value, 1.33, 4.2 and 17.3 striations are calculated for 1, 5 and 10 mixer elements, respectively, which agrees well with the data in Figure 6.

For particle dispersion in the stirred tank, the transect was located at two-thirds of the tank height, as shown in the first image of Figure 7. The transect resolution was based on the mean particle spacing, in the same way as for the micromixer data, giving a transect height, $\Delta z \cong 1$ mm, and a striation thickness threshold, $\Delta x \cong 1$ mm.

Figure 11 shows a rapid decay of maximum striation thickness during the initial stages of mixing, but no significant reduction in the scale of segregation after 10 impeller revolutions. Referring to Figure 7, and recalling that the only striations measured are for the black particles, not for the white spaces, the initial cluster sizes are less than one-tenth of the tank diameter, and the particles are rapidly dispersed throughout the tank: the first stage is dominated by macromixing with a rapid decay of the maximum striation thickness and CoV (Kukuková et al., 2008). During the later stages of turbulent mixing, accurate definition of a maximum striation thickness is difficult due to the sparse particle density at the smaller scales of segregation, and the fact that the particles disperse randomly in all directions, rather than through stretching distributions in the underlying velocity field.

The species concentration data in the last two test cases cover a continuous range of intensities due to the effects of molecular diffusion and turbulent eddies. As a result, the evaluation of striation thickness is based on a threshold concentration, instead of a threshold distance between tracking particles. For the smoke distribution test case, the saturated white smoke was assigned a concentration of 1 and the black background was assigned a concentration of 0. Several concentration thresholds were tested. By analogy with Equation (1), the f function was used to identify striations:

$$\begin{array}{ll} C > C_{\min} & f(x) = 1 \\ C \leq C_{\min} & f(x) = 0 \end{array} \tag{11}$$

where $C_{\min} = 0.2, 0.3, 0.4, 0.5$ and 0.6 and the mean concentration is close to 0.2, but varies from image to image. When the lower concentration limit is set too low, too much data are included and the striations blur together, making them hard to distinguish. In contrast, when the limit is set too high, visible striations of low concentration may not be detected. The maximum striation thickness for the smoke test case was measured on 15 vertical transects distributed along the streamwise direction, as shown in Figures 12 and 13.

Figure 12 shows the maximum striation thickness on 15 transects for the smoke distribution in Figure 8e. The maximum striation thickness gets higher as the concentration threshold drops. The smoke plume spreads as it flows from the jet outlet towards the right side of the picture, while the smallest scales of segregation get smaller and less distinct. The plume width, or the macroscale of segregation, is accurately captured with a concentration threshold of 0.2. Increasing the concentration threshold leads to the detection of the mesoscales of segregation, which

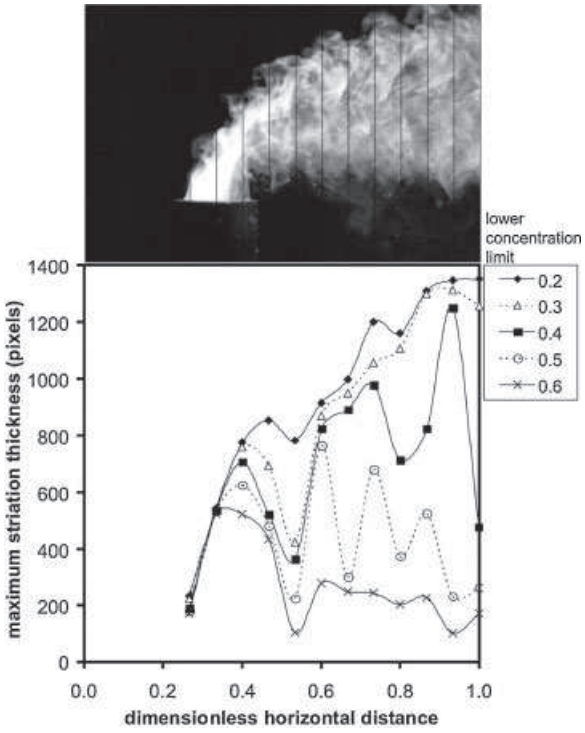

Figure 12. Maximum striation thickness on 15 transects for the smoke image in Figure 9e jet flow, showing a strong dependence on the concentration threshold. The image is 3008 pixels wide and 1960 pixels high. A greyscale intensity of 0.2 is equal to 82% of the mean concentration (0.24) for the whole image.

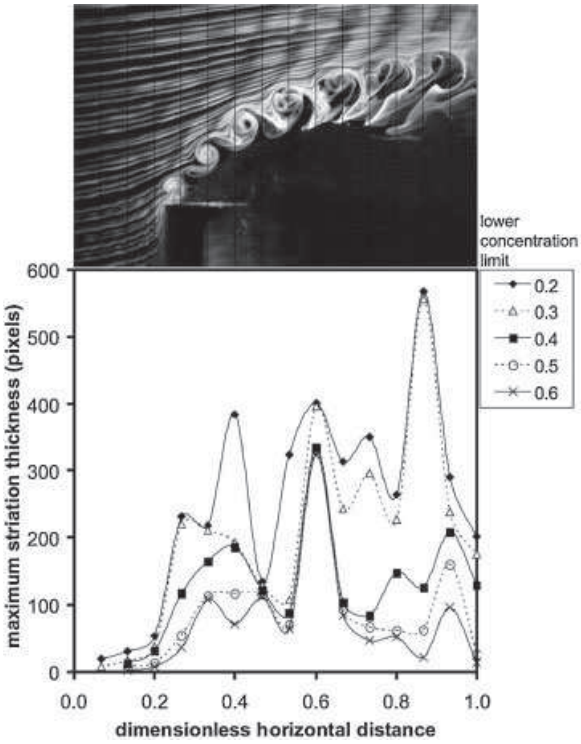

Figure 13. Maximum striation thickness on 15 transects for the smoke image in Figure 9d cross-flow, showing a strong dependence on the threshold concentration range. The image is 3008 pixels wide and 1960 pixels high. A greyscale intensity of 0.2 is 103% of the mean concentration (0.195) for the whole image.

decrease in size from left to right. The smaller scales of segregation are difficult to confirm because the striations are not very well defined in the image.

The maximum striation thickness for an image with clearly distinguishable striations is plotted in Figure 13. As in the previous case, the lowest concentration threshold accurately captures the macroscale of the smoke. In the first few transects where no large structures are present, the calculation gives the size of the visible small striations (15–20 pixels). Further along the image, the smallest striations cannot be detected by the maximum striation thickness measurement because the transects cut across much bigger smoke eddies. We conclude that if striations or any other small to moderate sized structures are to be detected using this method, the data set has to be free of structures bigger than the scale of interest. This can be accomplished by sub-sampling part of the image in a section that contains only striations, or only the mesosized structures.

To compare the results more directly with a homogeneous mixing field, two additional concentration thresholds were tested. A concentration threshold of 95% of the mean concentration $C_{\min} = 0.95\bar{C}$ was chosen in analogy to the mixing time criterion, and a limit of 200% of the mean concentration $C_{\min} = 2\bar{C}$ was tested in an attempt to reveal scales smaller than the macroscale, based on the observation that the initial results presented in the previous section tend to change from macroscale characterisation to measurement of smaller scales at around $C_{\min} = 0.4$, which is about 200% of the mean concentration. These limits were tested on a series of three images shown in Figure 14. Figure 14a shows the first image, originally part of Figure 9a. For this image, the transect is located at 2/15 of the image width, corresponding to the second transect in Figures 12 and 13. This transect location was chosen because only striations and no bigger structures cross this transect. The first enlarged sample, shown in Figure 14b, is 1/6 of the big image and contains only striations and no other structures. The third sample, shown in Figure 14c, is a 200×200 pixel sample showing three striations. The transects for both enlarged images are located at one half of the sample width. The maximum striation thicknesses for the 95% threshold were 34, 30 and 33 pixels, for the big, medium and small images, respectively. The calculated scales are very similar to each other for all analysed images. This shows that the maximum striation thickness on a transect accurately and consistently captures the largest scales in the data. For the 200% threshold, the maximum striation thicknesses were 13, 16 and 18 pixels, for the big, medium and small images, respectively. This measurement produces smaller scales than the 95% threshold and is well matched to the visual observation. The resulting length scales are obviously very sensitive to the concentration threshold. When the scale of smaller structures is needed, the data have to be re-sampled to isolate the small striations or eddies. There is no general recommendation for the selection of $C_{\min}$. Different thresholds reveal different scales in the data, so a meaningful $C_{\min}$ threshold has to be chosen for each problem.

The maximum striation thickness accurately captures the maximum length scale on a transect for either point or concentration data. The spatial resolution matches the mean particle spacing for particle data, and the pixel spacing for concentration data. The method is very fast to apply, but the results represent only a small sample of the population. Also, care must be taken to orient the transects perpendicular to the striations of interest and to let them pass through the worst mixed part of the mixing field. If smaller structures are to be captured, sub-sampling of the image

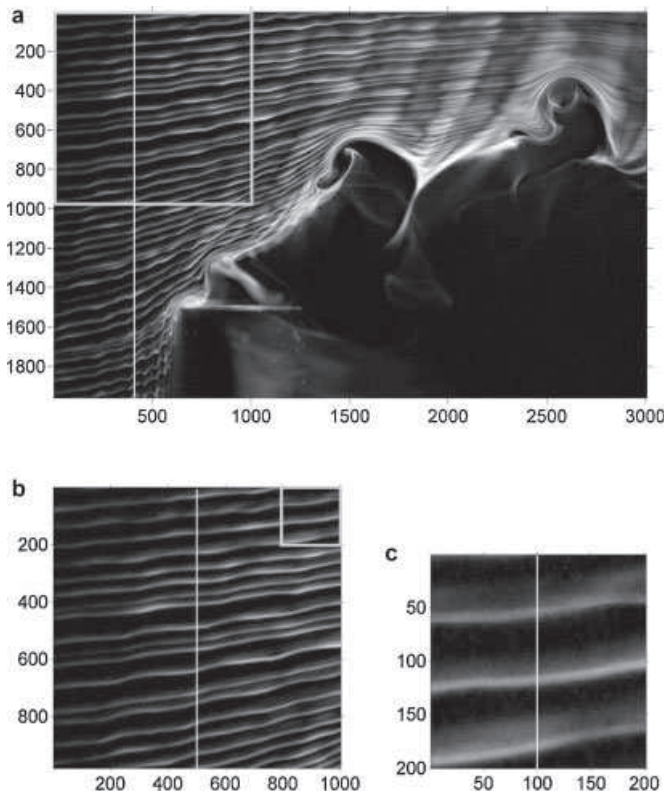

Figure 14. A series of enlarged smoke cross-flow images showing the transect locations.

may be required to isolate these structures. The maximum striation thickness is easiest to apply to point pattern data since the mean particle spacing for a perfectly regular distribution is easily determined. If concentration data are analysed, a concentration threshold has to be selected in order to define the striations and the results are very sensitive to this choice.

PNN

The PNN method is specifically suited to point pattern data and cannot be applied to concentration data. In this paper, it will be used for the micromixer and the stirred tank test cases. For both cases, a hexagonal grid of sampling points was used, as shown in Figure 3c. Figure 3d shows an example of the stirred tank particle data and Figure 3e illustrates the procedure used to find the nearest neighbours for each grid point.

For meaningful statistical analysis, the distribution of distances has to be normalised with some characteristic length scale. For mixing analysis, this scale should be independent of time or measurement resolution. The mean of the distribution changes with time and the grid spacing and the mean homogeneous particle spacing depend on the grid resolution and the number of particles, respectively. The maximum separation distance between two particles in the plane offers a physically meaningful measure, which is both time and resolution independent. In addition, the diagonal of a rectangle, or the diameter of a pipe could both be used so this normalisation can accommodate a range of mixing equipment. All PNN distances were normalised with the maximum separation distance and then multiplied by 100, giving distributions in terms of the percent of maximum separation for both geometries.

The effect of grid resolution was tested to verify the recommended selection of $k \approx \sqrt{n}$ (Diggle and Matern, 1980). For the stirred tank data, an image containing 32 000 particles was evaluated using sampling grids ranging from 130 grid points to 136 000 grid points. The mean PNN distance was consistent down to 512 grid points, and a smooth PNN distribution was obtained for grids of 8600 grid points and higher. To maximise the use of the particle tracking data, the number of grid points was matched to the number of particles for all subsequent calculations. The number of points in the grid was 2480 for the micromixer and ranged from 28 000 to 56 000 for the stirred tank to allow for the variation in the number of particles. The mean grid spacing for the micromixer is 2.7 μm and for the stirred tank, it ranges from 1.1 to 1.5 mm.

The normalised PNN distributions are compared with a Poisson distribution in Figures 15 and 16. The Poisson distribution has a mean and variance equal to the mean of the PNN distribution in all plots. Figure 15 shows the PNN distributions for the micromixer test case. Moving along the length of the micromixer, the distributions evolve from clustered to more random, which is illustrated by their approach to the random Poisson distribution. However, even at the micromixer outlet, the PNN distribution is more clustered than a random distribution. This accurately reflects the presence of visible striations at the end of the mixer in Figure 6. Notice that on the x-axis, the maximum measured separation drops from 40% of the diagonal to 10% of the diagonal over the length of the mixer.

Figure 16 compares the PNN distribution with the Poisson distribution for the stirred tank test case shown in Figure 7. As the mixing progresses, the PNN distribution approaches the random Poisson distribution, and the maximum measured separation decreases from 40% of the diagonal to less than 1% of the diagonal. At the beginning, the particle distribution is clustered, indicated by a wide distribution with a peak at a small distance. A skewed bell-shaped distribution appears at $Nt = 10$, which is the time when the particles have filled the volume of the tank. As the PNN distribution approaches the Poisson distribution, clustering is reduced and the particles are more evenly distributed at the smallest detectable scales.

In further studies, it might be interesting to investigate how the PNN distribution relates to the distribution of striation thicknesses in a sample area. This comparison was not completed in this work because the total number of measured striation thicknesses on a 1D transect did not provide enough data to represent the whole population of striation thicknesses in the 2D sample area.

The evolution of the index of dispersion is shown in Figures 17 and 18. The index of dispersion is the ratio of the population variance to the population mean. For a random distribution of particles, the index of dispersion is equal to one. For the micromixer test case in Figure 17, the curve decreases along the micromixer and tends to a value of one at the end of the micromixer as the particle distribution approaches a random state.

Figure 18 shows the index of dispersion curve for the stirred tank. The curve rapidly decreases and drops below a value of one after the first 10 time steps. Thereafter it decreases only slightly. These two parts of the curve indicate a two-stage process of mixing: the volume filling stage over the first 10 time steps, followed by a scale reduction stage in the later time steps (Kukuková et al., 2008). Index of dispersion values that are less than one show that the particle distribution quickly becomes more regular than a Poisson distribution.

The filtered point–particle variance, as defined in Equation (4), is shown in Figures 19 and 20 for several values of the filter threshold x_R. Figure 19 shows the evolution of the mixing quality in the micromixer expressed as the filtered PNN variance normalised by the variance at the inlet. Four PNN variance curves for x_R values of 0.5, 1.0, 2.5 and 5 μm correspond to approximately 20%,

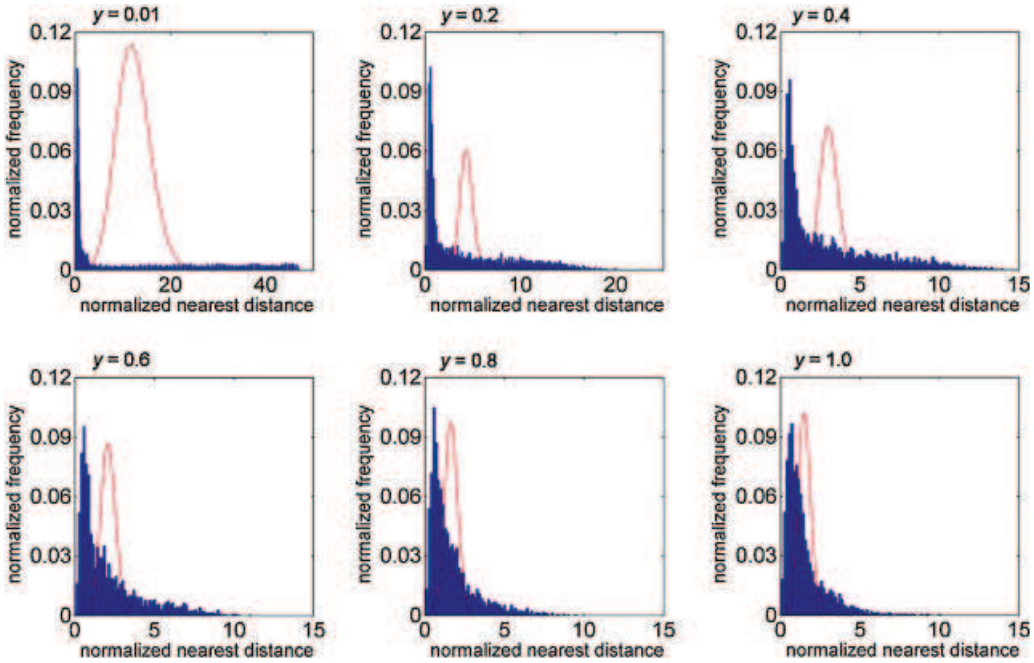

Figure 15. Comparison of the nearest distance distributions (histogram) with the Poisson distribution (curve) for several sampling planes along the micromixer.

40%, 100% and 200% of the mean grid spacing, respectively. As x_R increases, the PNN variance decreases because the criterion of what is considered close enough to the expected homogeneous distribution is more relaxed and it is easier to achieve the required scale of segregation.

Figure 20 presents the evolution of the filtered PNN variance over time in the stirred tank test case. The local point–particle variance is normalised by the point–particle variance at time equal to zero. Four x_R values of 0.5, 1.0, 1.5 and 3 mm, corresponding to approximately 33–50%, 67–100%, 100–150% and 200–300% of the mean grid spacing, were used. The percentage varies here since the number of particles—and therefore the number of grid points—varies slightly with each time step. The filtered variance shows a trend similar to the index of dispersion curve: a rapid decrease in the variance at the beginning, followed by a gradual decrease after 10 time steps. As expected, the PNN variance decreases as x_R increases and the scale of segregation requirement is relaxed. It can also be seen that the values of the filtered PNN variance for the turbulent stirred tank drop to a much smaller fraction of the initial variance than for the laminar micromixer.

The PNN method is only suitable for point pattern data. It is able to distinguish between segregated, clustered and regular

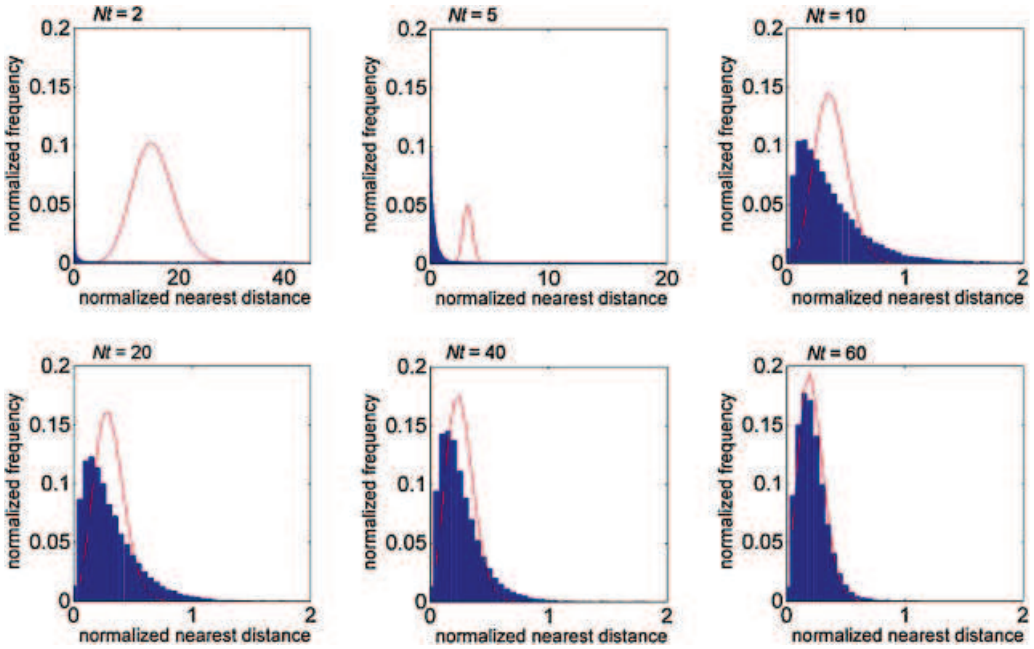

Figure 16. Comparison of the nearest distance distributions (histogram) with the Poisson distribution (curve) for each time step in the stirred tank.

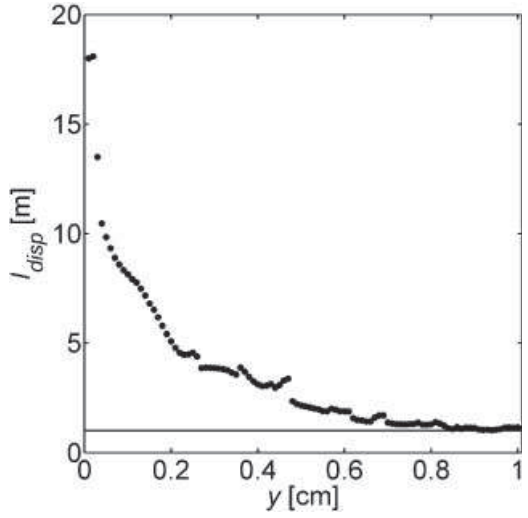

Figure 17. Evolution of the index of dispersion for the laminar micromixer.

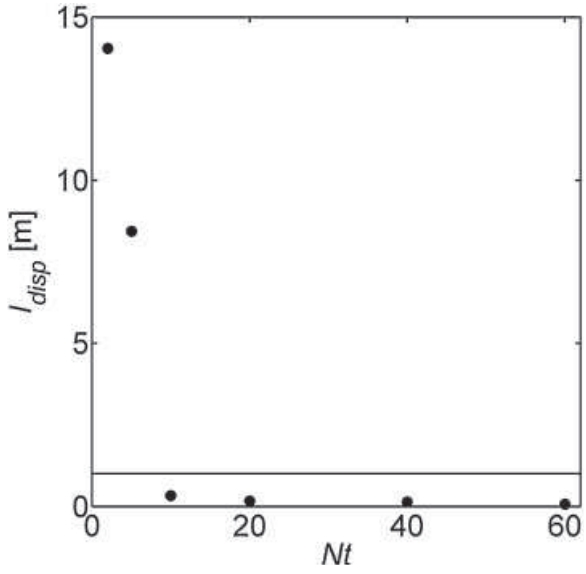

Figure 18. Evolution of the index of dispersion for the turbulent stirred tank.

distributions of particles. The index of dispersion provides a more quantitative measure of these characteristics, while the filtered PNN variance measures the uniformity of the distribution relative to a minimum acceptable scale of segregation. The advantage of the PNN method is that the results always represent the whole population and have an underlying physical meaning. The disadvantage of this method is that the calculation is time-consuming. The resolution of the PNN method ultimately depends on the number of tracking particles in the data set, and the matching of the grid to the number of particles, both of which increase the computational time.

Correlograms and Variograms

In order to use correlograms and variograms for point pattern data, concentrations would have to be calculated from quadrat sampling. Since it is known that quadrat sampling reduces the spatial resolution of the data, this approach is not recommended. Correl-

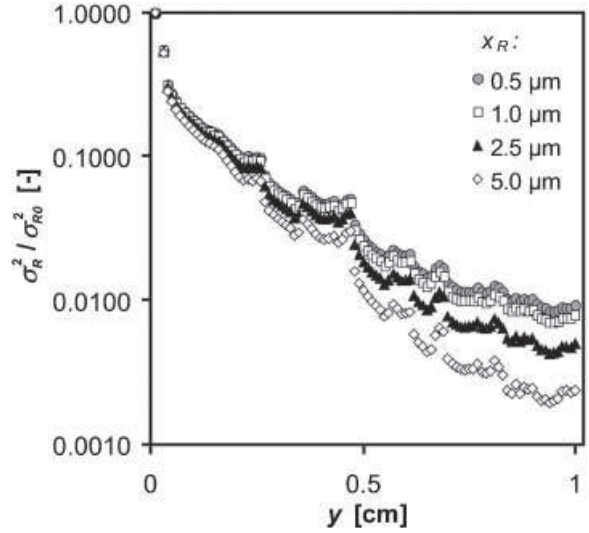

Figure 19. Normalised PNN variance for the micromixer test data showing the effect of the filter threshold, x_R. The mixing quality is expressed as the filtered PNN variance normalised by the PNN variance at the inlet.

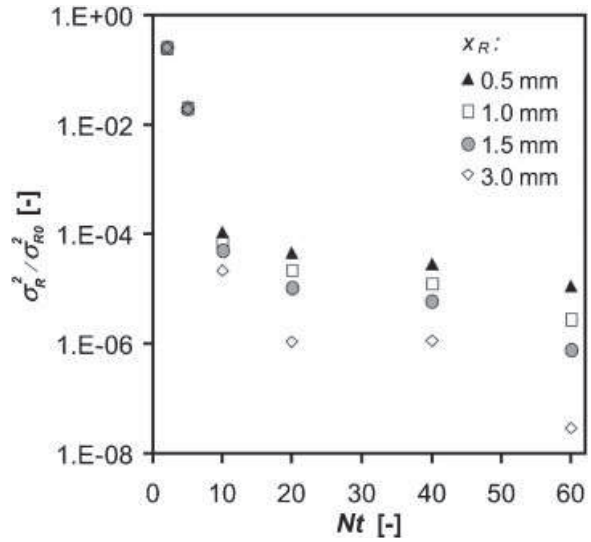

Figure 20. Normalised PNN variance for the stirred tank test data showing the effect of the filter threshold, x_R. The mixing quality is expressed as the filtered PNN variance normalised by the filtered PNN variance at time = 0.

ograms and variograms are best suited for full field concentration data.

The difference between the correlogram and the variogram was illustrated in Figure 4. We now return to a quantitative discussion of the plot, which shows the horizontal variogram and correlogram for the smoke image in Figure 8b cross-flow. The correlogram curve drops below zero and the variogram curve exceeds the value of one, indicating the presence of large-scale segregation. The original image reveals a large black area and another large unmixed area containing smoke striations. The evaluation of length scales from the correlogram is not defined for this kind of data because of the presence of macrosegregation and small oscillations due to local striations. Since large-scale segregation is common in the initial stages of mixing and the quantification of scales is desirable even for this type of mixing field, the

correlogram cannot be used consistently and only variogram results are discussed for subsequent calculations.

The length scale calculation from the variogram slope (Equation 10) involves a quantity P which characterises the proportion of minor species in the sample region. For the analysed images, the concentrations have a form of intensity with the scale going from zero to one, so P can be evaluated as the mean intensity in the image.

The variograms and the associated length scale calculations for the reactor test case were performed for all time steps and Reynolds numbers and representative results are shown in Figure 21. For both Reynolds numbers, the variograms approach one as time progresses, indicating little remaining correlation and thus good mixing. Both cases show a steadily increasing variogram curve, indicating large-scale segregation in the mixing field. Over time, the large-scale segregation diminishes for the higher Reynolds number case but remains in the laminar case. The persistent macroscale segregation, or lack thereof, is clearly visible in Figure 9. The variograms for the higher Reynolds number flow have periodic oscillations, which indicate an underlying periodicity in the data—in this case striations. Comparison of the horizontal and vertical variograms reveals a much bigger segregation in the vertical direction, where the variogram curves significantly exceed the value of one. In both directions, the macrosegregation reduces with time.

Horizontal and vertical length scales calculated from the variograms are shown in the bottom row of Figure 21. The length scales for the higher Re are about 10 times smaller than for the lower Re, which is expected. The scales increase initially as the clear fluid begins to fill the vessel, reach a peak, and decrease

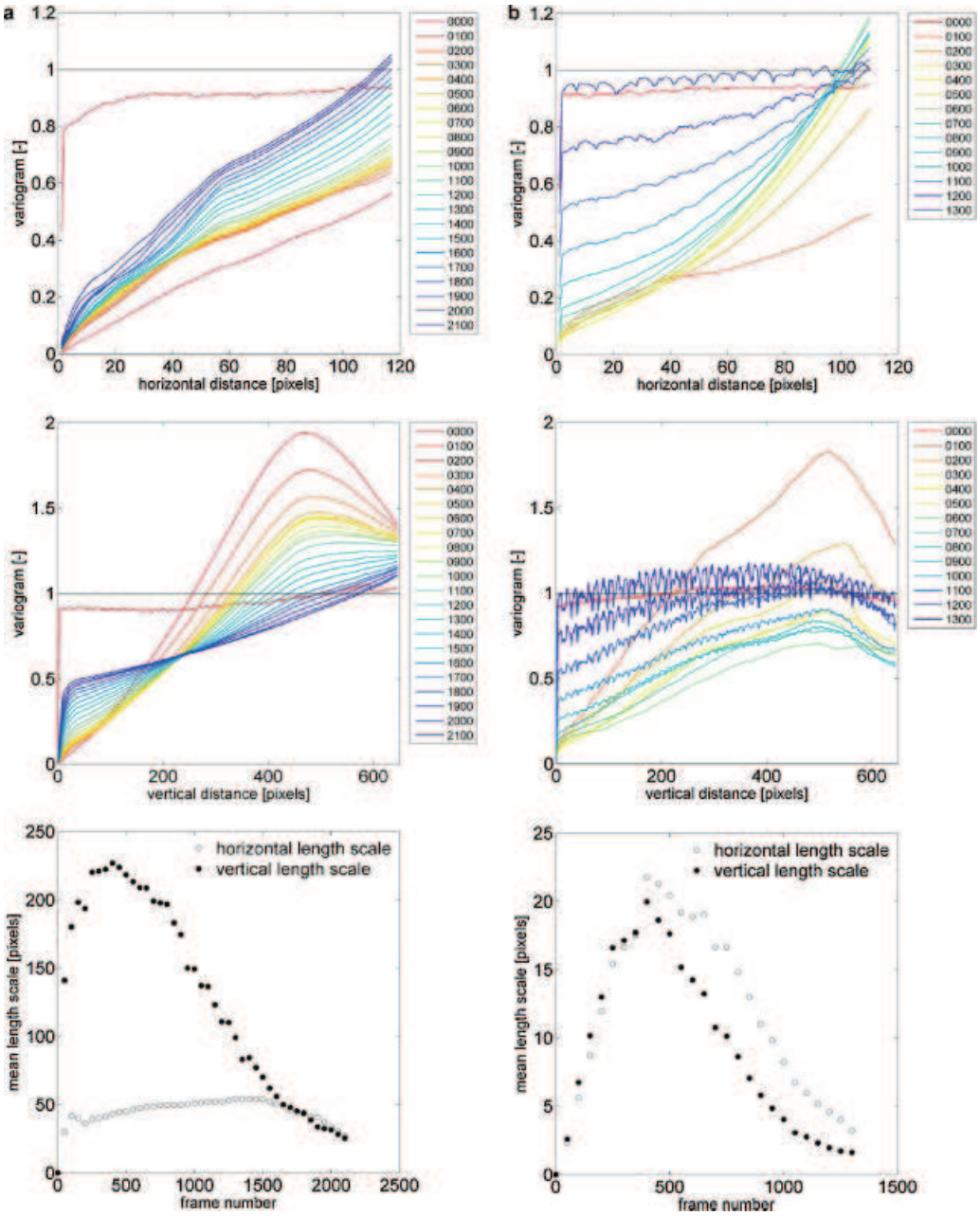

Figure 21. Reactor variograms and length scales; from top to bottom: horizontal variogram, vertical variogram and mean length scales; (a) Re = 17 and (b) Re = 1478.

as the injected fluid mixes with the contents of the reactor. The length scales at the end of the experiment are much lower for the higher Re case. The horizontal and vertical length scales are comparable for the higher Re flow, but for the laminar case, the vertical length scale is larger than the horizontal one. When the length scale is compared with the image and the pixel size of the image, some interesting results emerge. Comparing the horizontal and vertical length scales for the low Re case with the original image, the white area in frame 100 is about 190 pixels wide by 430 pixels high. The measured *average* length scale is 50 pixels in the horizontal direction and 200 pixels in the vertical direction. If the actual horizontal length scale is multiplied by the fraction of the vertical space taken up by the blob, the estimated mean length scale is 62, which approaches the variogram result of 50. Applying this same logic to the vertical length scale gives an estimate of 360 pixels, which is much larger than the reported result of 200 pixels. Similar comparisons can be applied to the rest of the images. The inevitable conclusion is that the mean length scale correctly tracks the progress over time to a better mixed image, but contains very little information about the complex mixing structures in the image, which necessarily contain a wide distribution of length scales. The length scale obtained from the variogram does not give a direct measure of the striation thickness.

Variograms for the smoke data are shown in Figure 22. The positive slope of the curves, which persists over most of the calculation range, arises from the large-scale segregation in the mixing field. The large black areas in the photographs dominate the results. The variograms also reveal periodicity in the concentration, which is most visible for the vertical cross-flow case. For some jet images, there is a slight periodicity of flow in the horizontal direction, but it is not as easily observed as the striations in the cross-flow case. This is due to the periodic repetition of smoke eddy structures, which can be seen in Figure 8a, c and d. For the laminar (Figure 8a) and turbulent (Figure 8e) smoke images, no periodicity can be either visually observed or detected using the variogram.

The horizontal and vertical mean length scales calculated from the initial slope of the variogram are presented in Figure 23. A first look at the figure reveals that the scales for the cross-flow images are always smaller than for the jet images. Indeed, the size of the smoke structures is smaller when the cross-flow is seeded with smoke, in contrast with the seeded jet flow. Further examination shows that the length scales in the horizontal direction are always bigger than in the vertical direction. For all the jet pictures, this is caused by the dimensions of the smoke cloud structure; its length is always bigger than its height. For the cross-flow image, this phenomenon arises because the horizontal direction cuts through the length of the smoke striations and the vertical direction cuts across their width.

Length scales calculated from variograms contain information about the mean macroscale of the concentration field. To investigate whether smaller scales can be captured, for example the width of smoke striations in the smoke images, the same enlarged images that were used for the maximum striation thickness analysis, shown in Figure 14, were used for the length scale calculation. The calculated vertical length scales were 11, 2.2 and 2.8 pixels for the big, medium and small images, respectively. The length scale was smaller for the enlarged images that contained striations only. The scale did not change much as the medium image was magnified further to show three striations only. These results show that smaller scales can be captured if a sub-sample containing

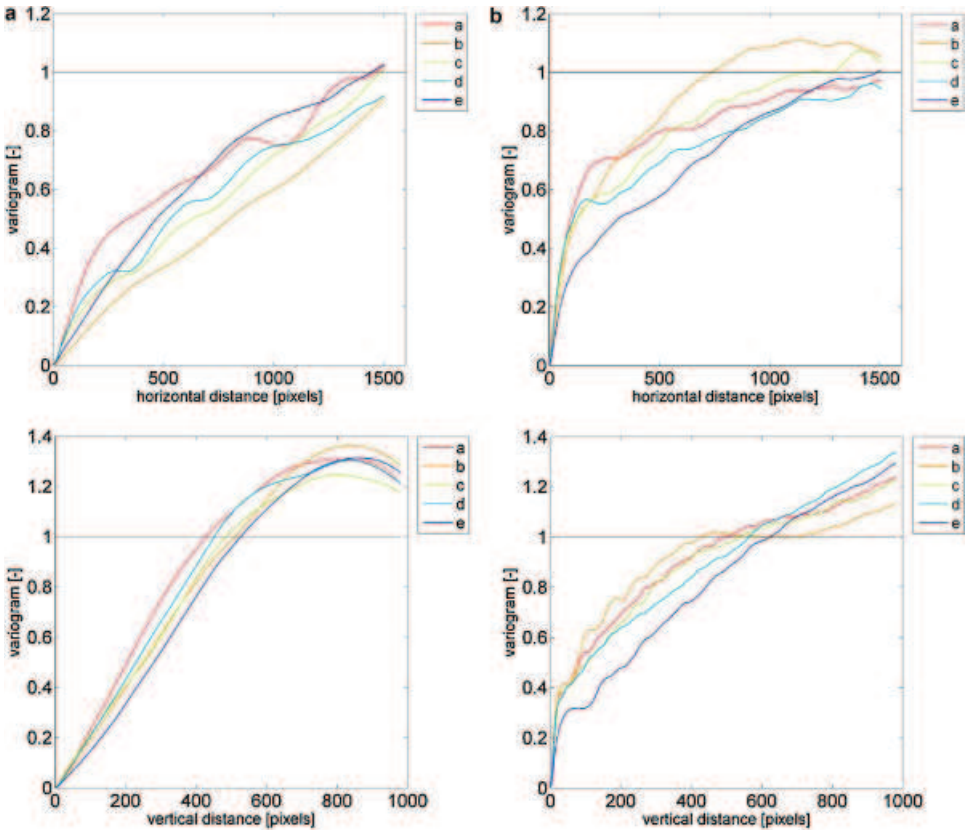

Figure 22. Horizontal (top) and vertical (bottom) variograms for the smoke data: (a) Jet flow and (b) cross-flow; results for data from Figure 9a–e, as shown in the legend.

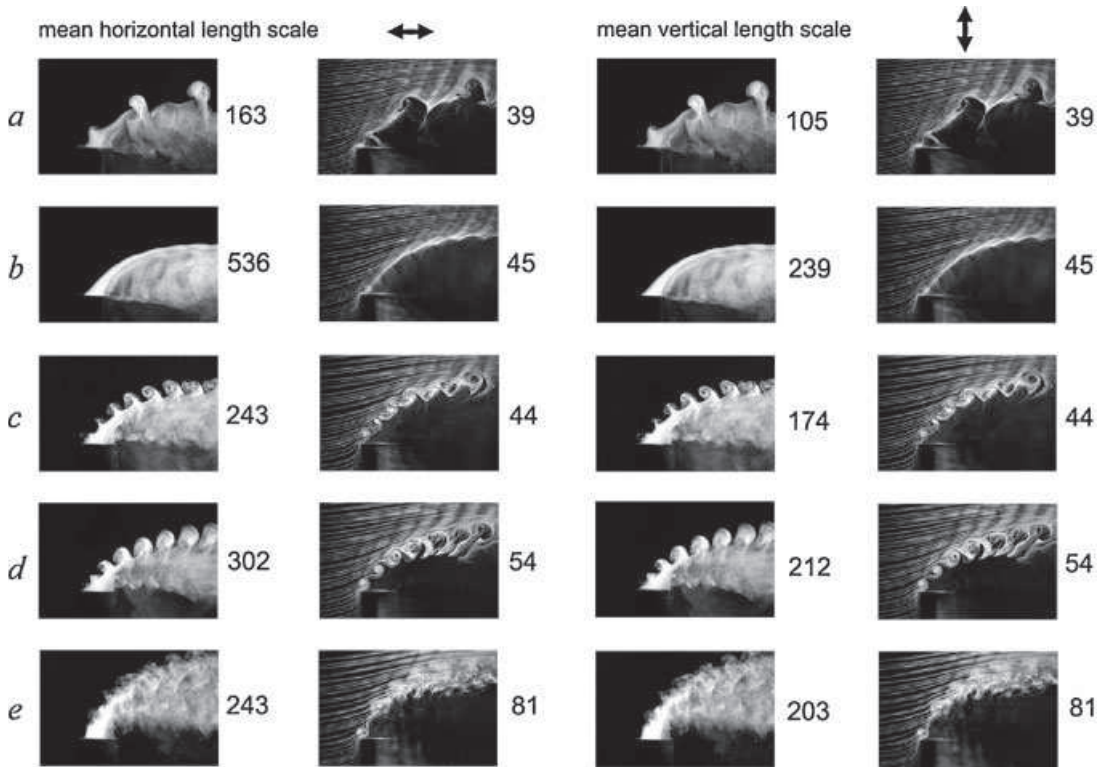

Figure 23. Mean horizontal and vertical length scales for the jet images.

only structures at the scale of interest is used for analysis, provided that a good data resolution is maintained. Comparing these variogram length scales with the maximum striation thicknesses for the same data clearly illustrates the difference between the two methods—the maximum striation thickness is sensitive to the concentration threshold, but accurately captures the striation size of 30 pixels; the variogram length scale of 2 pixels has no adjustable parameters, but also does not give the striation thickness directly.

The variogram is a useful tool for characterising the correlation or variability in concentration fields and has a resolution equal to the pixel resolution of the data. The variogram reveals both large-scale segregation and periodicity. The length scales calculated from variograms represent the average of the whole population in the concentration field, so sub-sampling is required if smaller structures in the mixing field are of interest. When interpreting the length scales, one must also bear in mind that they are not a direct measure of the striation thickness, or even an area averaged striation thickness. No simple method has yet been proposed to extract a distribution of length scales directly from variogram data. In comparison to the maximum striation thickness and PNN calculations, this method is moderately fast.

CONCLUSIONS

The objective of this work was to examine four methods of measuring the scale of segregation and to test their application to 2D fields of mixing data: the maximum striation thickness on a transect, PNN distributions, the correlogram and the variogram. Two types of data were used to evaluate the measurement methods: particle tracking data and concentration field data, with two test cases of each type. The particle tracking data were obtained from laminar mixing of particles in a staggered herringbone micromixer and turbulent dispersion of particles in a stirred tank. The concentration field data were for a jet in cross-flow and for a concentration step change experiment in a continuous flow industrial reactor.

The methods were compared and evaluated in order to determine their strengths and limitations for the analysis of mixing data. Five questions were addressed during the evaluation of the four measures:

1. What type of data is the method suitable for?
2. What information does it provide?
3. Are the results physically meaningful?
4. What is the smallest scale of mixing resolved by the method?
5. How fast is the calculation?

The answers to this set of questions are conveniently summarised in Table 1, followed by a more detailed discussion of each of the criteria.

The suitability of a measurement method varies for different types of data. The maximum striation thickness on a transect is easiest to apply to point pattern data since the sharp striation interfaces are easily determined. If concentration data are analysed, a concentration threshold has to be selected in order to define the striations and the results are very sensitive to this choice. The PNN method is only suitable for point pattern data and cannot be used for concentration data. Both the variogram and correlogram are useful for characterising concentration data, however, only the variogram can be used to determine length scales from data containing large-scale segregation or periodicity. Because this type of data is common in today's mixing research, correlogram calculations were not pursued.

The methods provide scale measurements in different forms. The maximum striation thickness accurately captures the maximum length scale on a transect. The PNN method is able

Table 1. Comparison of the four methods for measuring the scale of segregation

	Maximum striation thickness on a transect	PNN	Correlogram	Variogram
What type of data is the method suitable for?	Location data (point patterns) concentration data (not so easy)	Location data (point patterns)	Concentration data; no large scale segregation, no periodicity	Concentration data
What information does it provide?	Maximum length scale; sampled data	Clustering character, closeness to homogeneous distribution; whole population	N/A	Integral length scale; whole population
Are the results physically meaningful?	Exact length scale	Exact distance distribution	N/A	Proportional to real scales
What is the smallest scale of mixing resolved by the method?	Mean inter-particle spacing	Mean grid spacing	N/A	Measured data spacing (e. g. 1 pixel)
How fast is the calculation?	Fast, 7 s[a]	Time consuming, 9 min[a]	N/A	Moderately fast, 6 min 25 s[a]

[a] The calculation times are for one frame, calculated in Matlab R 2009a using the AMD Athlon 64 processor, 2.41 GHz and 2 GB RAM.

to distinguish between segregated, clustered and regular distributions. The index of dispersion calculated from the PNN distributions provides a more quantitative characterisation of the distribution of the population. The filtered PNN variance measures the uniformity of the distribution relative to a reference scale of segregation, x_R. The variogram is a useful tool for characterising the correlation or variability in concentration data and can reveal both large-scale segregation and periodicity. The length scales calculated from variograms represent a proportional average of the whole data field.

The physical meaning of the results depends on the quality of sampling. The maximum striation thickness on a transect represents only a small sample of the population, so to get meaningful results, care must be taken to orient transects perpendicular to the striations of interest and to let them pass through the worst mixed part of the mixing field. If smaller structures need to be captured, sub-sampling of the image may be required. The PNN distributions always represent the whole population and have an underlying physical meaning provided enough tracking particles are used to resolve the scales of interest, and the number of grid points is matched to the number of particles. The index of dispersion provides a measure of departure from a random distribution for the whole population. The filtered PNN variance uses a sample of the population, which depends on the filter size x_R. Increasing the filter size relaxes the homogeneity criterion. The length scales calculated from variograms represent the average of the whole population in the data field, so sub-sampling is required if smaller structures in the mixing field are of interest. When interpreting the variogram length scales, one also has to bear in mind that they are not exact length scales but proportional length scales, and no simple method has yet been proposed to extract a distribution of real length scales from variogram data.

The smallest length scale that can be obtained from the striation thickness calculation is slightly smaller than the mean particle spacing that is used to define the striation threshold. For complex data sets, sub-sampling of data is needed to measure the size of small structures. For the PNN distributions, the smallest scales are given by the mean grid spacing. The minimum scale of the variogram measurement is fixed by the image resolution.

The speed of calculation is directly proportional to the size of the data set and the number of operations for each frame. The maximum striation thickness on a transect calculation is the fastest because it involves just one or a few line samples of the data. The PNN calculations were the most time consuming because the number of grid points was matched to the number of particles and the distances from all grid points to all particles were calculated. The variogram calculations were moderately fast compared to the other methods. Both the PNN and the variogram algorithms could be optimised to get faster results, but in both cases the computations were fast enough that this was not deemed necessary.

This study provides a toolkit of methods for length scale characterisation, together with benchmarks for the use and limitations of each tool. The calculation algorithms for each method are available as supplementary material from the Journal or on request to the corresponding author.

NOTATION

A	sample region
C	concentration (mol/L or 1)
$\bar{C}$	mean concentration (mol/L or 1)
$C_i(x)$	concentration at location x (mol/L or 1)
C_{imp}	impeller off-bottom clearance (m)
C_{is}	standardised concentration value at location x
C_{min}	lower limit of the concentration threshold (mol/L or 1)
CoV	coefficient of variance
d_g	micromixer groove depth (μm)
D	impeller diameter (m)
D_{pipe}	pipe diameter (m)
dx	grid spacing in x direction (m)
dxz	length of the hexagon side in the sampling grid (m)
dz	grid spacing in z direction (m)
$f(x)$	function for distinguishing striations
h	data separation distance (m, pixels)
H	micromixer height (μm)
k	number of grid points in one direction
m	number of grid points or nearest distances
n	number of particles in area A, number of mixer elements
$N(h)$	total number of pairs of data separated by distance h
Nt	number of time steps/impeller revolutions
i	measurement location number
I_{disp}	index of dispersion (m)
K_0	number of fluid divisions in a mixer element

L_D mean length scale calculated from the correlogram (m, pixels)
L_V mean length scale calculated from the variogram (m, pixels)
P proportion of species of interest in the sample region
Re Reynolds number
Re_d jet Reynolds number
$R_x(h)$ coefficient of correlation at separation distance h
T tank diameter (m)
w_g micromixer groove width (μm)
W micromixer width (μm)
x, y, z Cartesian coordinates (m)
x_G mean grid spacing (m)
x_i nearest distance for ith grid point (m)
$\bar{x}_i$ mean PNN distance (m)
x_R PNN variance filter threshold (m)
Δx particle separation threshold (m)
Δz transect height (m)

Greek Letters

$\gamma_x(h)$ variogram at separation distance h
σ^2 variance (mol^2/L^2 or 1)
σ_R^2 filtered PNN variance (m^2)
σ_R^2 filtered PNN variance at the micromixer inlet or at time = 0 (m^2)
ξ x coordinate of the point on the $R_x(h)$ curve where the curve crosses 0 (m)

ACKNOWLEDGEMENTS

The authors wish to thank Jos Derksen, Hugo Hartmann, Lorenz W. Sigurdson, Graeme M. G. Watson and an anonymous corporate colleague for providing the mixing test case data sets, which were used in this work.

REFERENCES

Atiemo-Obeng, V. A. and R. V. Calabrese, "Rotor Stator Mixing Devices," in "Handbook of Industrial Mixing: Science and Practice," E. L. Paul, V. A. Atiemo-Obeng and S. M. Kresta, Eds., John Wiley & Sons, Inc., New Jersey (2004), pp. 479–506.

Aubin, J., D. F. Fletcher and C. Xuereb, "Design of Micromixers Using CFD Modelling," Chem. Eng. Sci. **60**, 2503–2516 (2005).

Bałdyga, J. and J. R. Bourne, "Turbulent Mixing and Chemical Reactions," John Wiley & Sons, Inc., New York (1999), pp. 890.

Bennington, C. P. J., "Mixing in the Pulp and Paper Industry," in "Handbook of Industrial Mixing: Science and Practice," E. L. Paul, V. A. Atiemo-Obeng and S. M. Kresta, Eds., John Wiley & Sons, Inc., New Jersey (2004), pp. 1187–1246.

Carle, S. F. and G. E. Fogg, "Transition Probability-Based Indicator Geostatistics," Math. Geol. **28**, 453–476 (1996).

Chu, L. Y., A. Utada, R. Shah, J. W. Kim and D. Weitz, "Controllable Monodisperse Multiple Emulsions," Angew. Chem. Int. Ed. **46**, 8970–8974 (2007).

Cottam, G. and J. T. Curtis, "A Method for Making Rapid Surveys of Woodlands by Means of Pairs of Randomly Selected Trees," Ecology **30**, 101–104 (1949).

Danckwerts, P. V., "The Definition and Measurement of Some Characteristics of Mixtures," Appl. Sci. Res. Sect. A: Mech. Heat Chem. Eng. Math. Methods **3**, 279–296 (1952).

Deutsch, C. V., "Geostatistical Reservoir Modelling," in "Applied Geostatistics Series," A. G. Journel, Ed., Oxford University Press, New York (2002), pp. 376.

Diggle P. J., "Statistical Analysis of Spatial Point Patterns," Oxford University Press, New York (2003), pp. 159.

Diggle, P. J. and B. Matern, "On Sampling Designs for the Study of Point-Event Nearest Neighbor Distributions in R2," Scand. J. Stat. **7**, 80–84 (1980).

Etchells, A. W. and C. F. Meyer, "Mixing in Pipelines," in "Handbook of Industrial Mixing: Science and Practice," E. L. Paul, V. A. Atiemo-Obeng and S. M. Kresta, Eds., John Wiley & Sons, Inc., New Jersey (2004), pp. 391–478.

Gullett, B. K., P. W. Groff and L. A. Stefanski, "Mixing Quantification by Visual Imaging Analysis," Exp. Fluids **15**, 443–451 (1993).

Hartmann, H., J. J. Derksen and H. E. A. Van den Akker, "Numerical Simulation of a Dissolution Process in a Stirred Tank Reactor," Chem. Eng. Sci. **61**, 3025–3032 (2006).

Johnson, B. K. and R. K. Prud'homme, "Chemical Processing and Micromixing in Confined Impinging Jets," AlChE J. **49**, 2264–2282 (2003).

Kukukova, A., J. Aubin and S. M. Kresta, "A New Definition of Mixing and Segregation: Three Dimensions of a Key Process Variable," Chem. Eng. Res. Des. **87**, 633–647 (2009).

Kukuková, A., B. Noël, S. M. Kresta and J. Aubin, "Impact of Sampling Method and Scale on the Measurement of Mixing and the Coefficient of Variance," AlChE J. **54**, 3068–3083 (2008).

Lacey, P. M. C. and F. Mirza, "Study of Structure of Imperfect Mixtures of Particles 2. Correlational Analysis," Powder Technol. **14**, 25–33 (1976).

Liu, S. P., A. N. Hrymak and P. E. Wood, "Drop Breakup in an SMX Static Mixer in Laminar Flow," **83**(5), 793–807 (2005).

Mohr, W. D., R. L. Saxton and C. H. Jepson, "Mixing in Laminar-Flow Systems," Ind. Eng. Chem. **49**, 1855–1856 (1957).

Muzzio, F. J., P. D. Swanson and J. M. Ottino, "The Statistics of Stretching and Stirring in Chaotic Flows," Phys. Fluids A: Fluid Dyn. **3**, 822–834 (1991).

Nathan, G. J., J. Mi, Z. T. Alwahabi, G. J. R. Newbold and D. S. Nobes, "Impacts of a Jet's, Exit Flow Pattern on Mixing and Combustion Performance," Prog. Energy Combust. Sci. **32**, 496–538 (2006).

Newbold, G. J. R., G. J. Nathan, D. S. Nobes and S. R. Turns, "Measurement and Prediction of NO_x Emissions From Unconfined Propane Flames From Turbulent-Jet, Bluff-Body, Swirl, and Precessing Jet Burners," Proc. Combust. Inst. **28**, 481–487 (2000).

Watson, M. G. G., "The Structure and the Controlled Relaminarisation of Low Momentum Elevated Jets-in-Crossflow," MSc Thesis, University of Alberta, Edmonton (2007).

Watson, G. M. G. and L. W. Sigurdson, "The Controlled Relaminarisation of Low Velocity Ratio Elevated Jets-in-Crossflow," Phys. Fluids **20**, 15 (2008).